Fabrication of Novel Transparent Co_3O_4- TiO_2 nanowires p-n heterojunction diodes for Multiband Photodetection Applications

Bijit Choudhuri[1], Aniruddha Mondal[2,*], Shyam Murli Manohar Dhar Dwivedi[2]

Mohamed Henini[3]

[1]Department of Electronics and Communication Engineering, National Institute of Technology Agartala, Jirania -799046, India

[2] Department of Physics, National Institute of Technology Durgapur, Durgapur-713209, India

[3]School of Physics and Astronomy, The University of Nottingham, Nottingham, NG7 2RD, United Kingdom

*E-mail: aniruddhamo@mail.com, Phone number: +91-9434789024

Abstract:

Axial Co_3O_4 - TiO_2 heterojunction nanowires (NWs) were synthesized by glancing angle deposition (GLAD) technique. The p-n heterojunction showed excellent rectification ratio of 2.26×10^2 at ± 3.4 V. The forward turn on voltage of 1.5 V in the dark was reduced to 1 V under white light excitation on the device. The diode showed a maximum half-wave rectification efficiency of 7.77% at 200 Hz frequency operated with maximum ± 10 V. The device showed maximum peak responsivity of 4.01 A/W and internal gain of 13.1 at 380 nm wavelength. The detectivity was calculated to be 2.82×10^{11} and 1.69×10^{11} Jones and the noise equivalent power was estimated to be 14.9 and 24.8 pW at 380 and 620 nm wavelength, respectively. The device spatial response showed sharp transition with rise and fall time of ~ 0.17s and 0.21s, respectively.

Keywords:

Semiconductors, optical materials, oxide materials, thin films, electron-phonon interactions, photoconductivity and photovoltaics

1. Introduction

Metal oxide semiconductors have become dominating materials in the field of nanoscience research due to higher efficiency, diverse properties (ferromagnetic, ferroelectric, supercapacitive, semiconducting and superconducting) and relatively easy preparation methods [1-3]. The electrical, optical, physical, chemical and other properties of the oxide semiconductors can be altered very easily as per requirement by simply tuning the bandgap structure through doping impurities, morphology, Schottky or Ohmic contact formation etc. [4-6]. The majority of these oxide semiconductors are inherently n-type such as TiO_2, ZnO, SnO_2, Fe_2O_3, In_2O_3 etc. [7] due to the interstitial defects and related oxygen vacancies. Considerable efforts have been paid to synthesize transparent homojunctions by synthesis of p-type counterpart of the mentioned material. However, due to the instability of the p-type oxides, fabrication of the transparent homojunction is still a challenge to fabricate. A p-n heterojunction is a junction between two materials with different bandgaps. These structures have the superiority to prevent the generated electron-hole pairs to recombine due to the presence of bandgap discontinuity at the p-n interface. It is important to mention that there are some inherently p-type oxide semiconductors such as Cr_2O_3, CuO, NiO, Co_3O_4, Mn_3O_4 etc [8]. Several heterojunction combinations of these materials have been studied vastly for gas sensing purposes. Among these materials Co_3O_4 has a direct bandgap varying between 2 to 2.8 eV which falls in the visible region [9-11], and is able to absorb the visible portion of solar radiation spectrum. Co_3O_4 and its heterojunctions with TiO_2 may be able to reveal a wide range of solar spectrum from UV to near infrared region. Research on nanowires nowadays are expanding at a very rapid rate due to some of their outstanding properties such as guidance of light owing to high refractive index, ability to form interpenetrating co-axial

and longitudinal heterojunction interface and mostly for strong light trapping [12] on the front panel of the optoelectronic devices. Previously, synthesis of Co_3O_4 was reported by solvothermal process [13], hydrothermal process [14], sol-gel method [15], and oxidation of cobalt [16].The Glancing Angle Deposition (GLAD) method is a cost effective technique to grow different nanostructure morphology by simply altering the substrate azimuthal rotation speed, angle of deposition and rate of deposition [17]. Hence, the investigation of optoelectronic properties of GLAD synthesized Co_3O_4 - TiO_2 longitudinal nanowire heterojunctions is carried out.

In this article, we report the synthesis of Co_3O_4 - TiO_2 longitudinal heterojunction nanowires grown by GLAD technique. The absorption and transmission spectra were measured and analyzed. Room and low temperature measurements of the current density-voltage characteristics have been made and half wave rectification efficiency of the p-n heterojunctions and ideality factors were calculated, respectively. In addition, the spectral responsivity and spatial response measurements of the detector were performed.

2. Experimental

2.1. Synthesis of Co_3O_4-TiO_2 nanowire heterojuntion (NWH)

Co_3O_4 pellets were prepared from Co_3O_4 nanopowder (Sigma Aldrich-637025) without using any binder by a KBr hydraulic press under a pressure of 60 Kg/cm^2 for 10 minutes duration. The formed pellets were then sintered inside a quartz tube furnace (GSL-1700X, MTI, USA) in open air condition at 600° C for 30 minutes using even heating and cooling ramp of 4°C/min. These pellets were used to deposit Co_3O_4 nanowires (NWs) inside an electron beam evaporator. Prior to the deposition, n-Si <100> (30 Ω-cm) substrates were cleaned using trichloroethylene, methanol, acetone, and a solution of hydrofluoric acid and de-ionized water at 1:50 volume ratio. A 50 nm thick TiO_2 film was grown on the substrate using an electron

beam evaporator (BC-100, Hind High vacuum Co. (p) Ltd.) at a base pressure of 10^{-6} mbar. Next, 250 nm long perpendicular TiO_2 NWs were grown inside the chamber of the same e-beam evaporator using GLAD technique. The substrate holder was kept at a distance of 24 cm from the evaporated material source at an orientation of 85° with respect to the perpendicular line between the source and the substrate, having an azimuthal rotation of 10 rpm. This was followed by 250 nm Co_3O_4 NWs deposited from Co_3O_4 pellet source using the same experimental setup mentioned above. Finally, 30 nm thick gold (Au) was evaporated to form the top electrode using an aluminium mask with hole area of 1.77×10^{-6} m^2.The growth rate was kept constant at 1.2 Å s^{-1} for deposition of TiO_2, Co_3O_4 and Au.

2.2 Characterization

Scanning electron microscopy (SEM) (Sigma, Zeiss) and energy dispersive X-ray (EDX) (ZEISS EVO-MA 10) analysis were performed on the samples to investigate the morphological orientation. The transmission electron microscopy (TEM) (JEM-2100, 200 kV, Jeol) investigation with selected area electron diffraction analysis were carried out on the samples. A UV-Visible near-infrared optical absorption spectrophotometer (Lambda 950, Perkin Elmer) was used to measure the optical absorption and transmission spectra of the samples. The p-n junction half wave rectification was observed by connecting the junction diodes in series with a 1 MΩ resistance and using a digital storage oscilloscope (TBS1062, Tektronix). The current density (J) vs. voltage (V) and photocurrent measurements were performed using a Keithley 2401 source-measure unit, a 300 W xenon arc lamp and a monochromator (Sciencetech Inc. Canada) in open beam configuration. The transient time response of the device was measured under white light on-off irradiation. The temperature dependent J-V characteristics from 50K-300K were measured using a closed cycle helium cryostat (Advanced Research System Inc.).

3. Results and discussion

3.1. Structural Depiction

Fig. 1 shows the top view SEM micrograph of Co_3O_4-TiO_2 nanowire heterojuntion (NWH) synthesized on indium tin oxide (ITO) coated glass (Fig. 1a) and n-Si substrates (Fig. 1b). The images show that the NWs, grown on ITO coated glass and n-Si substrates, have typically diameter ranges of 40-50 nm and 40-60 nm, respectively. Fig. 1c reveals the EDX spectrum for the Co_3O_4-TiO_2 NWH. The EDX spectrum verifies the presence of titanium (Ti), cobalt (Co) and oxygen (O_2) in the prepared samples.

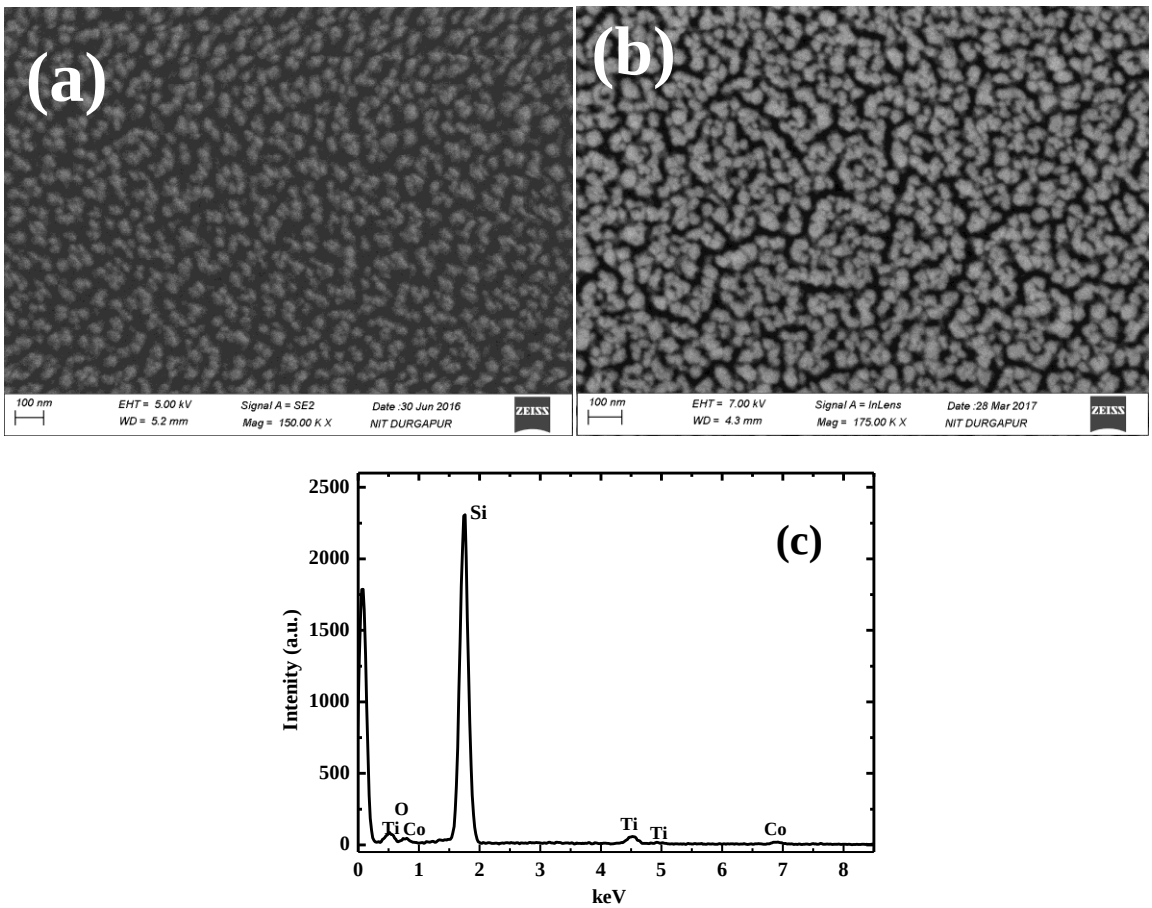

Fig. 1: Top view SEM images of TiO_2-Co_3O_4 NW arrays prepared on (a) ITO coated glass and (b) n-Si substrate; (c) EDX spectrum

The morphology of the NWH has been investigated separately using TEM characterization technique to verify the formation of perpendicular NWs. The color contrast in the cross-

section micrograph confirms the formation of the heterojunction between TiO_2 and Co_3O_4. The observation reveals that TiO_2 NWs have a diameter of ~20 nm at bottom which gradually increases to 50 nm at the interface of TiO_2 and Co_3O_4.The top diameter of Co_3O_4 was measured to be 40 nm. The height of TiO_2 and Co_3O_4 were 170 nm and 90 nm, respectively. The selected area electron diffraction (SAED) analyses of Co_3O_4 show its amorphous nature (Fig. 2 c, d) with diffuse concentric rings, while TiO_2 shows polycrystalline nature with bright concentric spotty rings having typical d spacing of 0.21 nm attributed to (210) plane (Fig. 2e, f) of rutile TiO_2 [18]

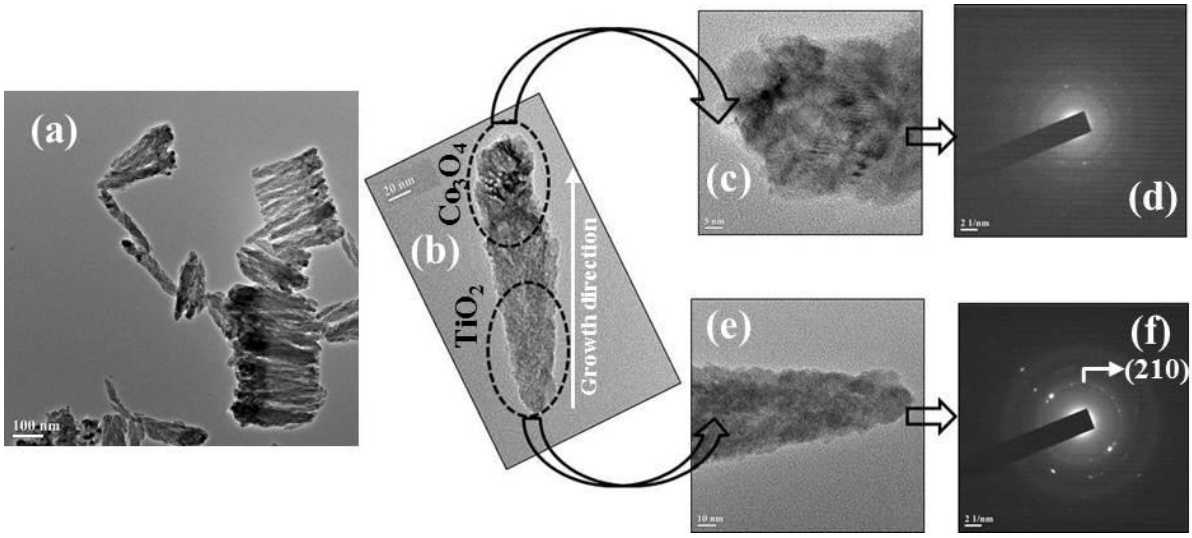

Fig. 2. TEM images of the Co_3O_4-TiO_2 NWH (a) NWs arrays, (b) individual NW, (c) magnified view of upper portion (Co_3O_4) of the heterojunction, (d) SAED of Co_3O_4 section, (e) magnified view of lower portion (TiO_2) of the heterojunction, (f) SAED of TiO_2 section

3.2. Optical Characterization

Fig. 3a shows the room temperature UV-Vis optical absorption spectra for TiO_2-Co_3O_4 heterostructure deposited on ITO coated glass substrate. The peak at 380 nm may be due to the main band transition in TiO_2 [19] whereas the small shoulder at 425-445 nm can be assigned to the absorption via intrinsic surface states [20]. The broad peak at 620 nm may be

ascribed to the main band transition in Co_3O_4 [10]. The $(\alpha hv)^2$ vs hv characteristics for TiO_2-Co_3O_4 heterostructure on ITO coated glass and n-Si substrates are represented in Fig. 3b where α is the absorption coefficient and hv is the photon energy. Extrapolation of linear part of the spectra yielded band gap values of 3.29 eV, 2.75 eV, 2.25 eV and 1.6 eV for ITO coated glass substrate based samples and 3.28 ev and 2.23 eV for n-Si substrate based samples. Among them, 3.29 and 3.28 eV are due to the main band transition in TiO_2 [19] whereas the value at 2.75 eV (450.9 nm) is very close to the reported value of TiO_2 (450 nm) [21]. The 2.25 eV and 2.23 eV energy may be attributed to the band to band transitions due to oxygen to Co (II) and Co (III) metal to ligand charge transfer [22], and the 1.6 eV band is due to indirect bandgap transition in Co_3O_4 [23]. Fig. 3c shows the room temperature optical transmittance spectra for the TiO_2-Co_3O_4 heterostructure. In a range between 375 nm - 800 nm, the heterostructure allowed 73% photon to pass through it.

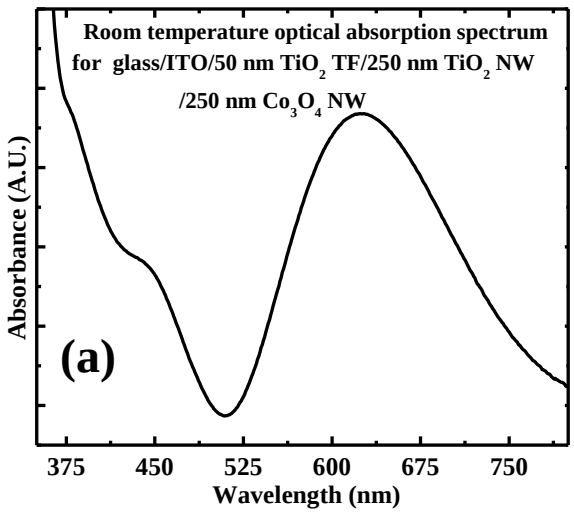

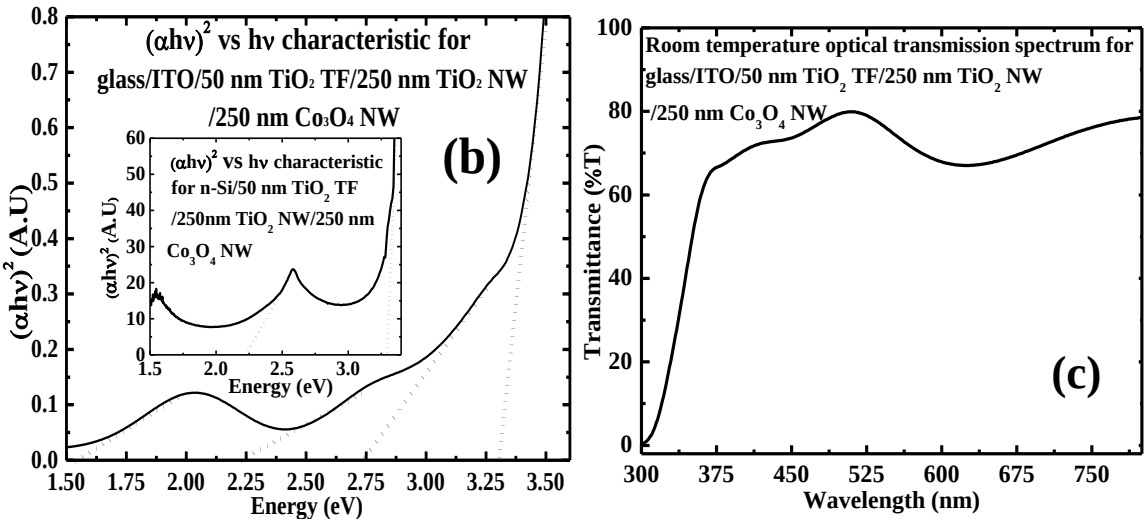

Fig. 3: UV-Vis optical spectra of TiO_2- Co_3O_4 NWs (a) absorption, (b) $(\alpha h\nu)^2$ versus energy curve for sample prepared on ITO coated glass and n-Si substrate (inset) (c) transmission

3.3. Co_3O_4 - TiO_2 heterostructure based p-n diode characteristics

The axial Co_3O_4 - TiO_2 heterojunction NWs based diode (HND) is fabricated on TiO_2 TF coated n-Si substrate as shown schematically in Fig. 4a. A transparent top Ohmic contact was made of Au on Co_3O_4 NWs and Al was used as back contact on the Si substrate. James E. Moore et al reported a conduction band offset of 0.4 eV at the CdS/CIGS interface [24] and 0.15 eV for a-Si:H/c-Si heterojunction solar cell [25]. We have calculated the conduction band offset of 0.4 eV and valence band offset of 0.64 eV for the Co_3O_4 - TiO_2 heterointerface (Fig.4b), where the electron affinity of Co_3O_4 was considered as 1.99 eV using Vegard's law from the electron affinity of CoO_n [26].This band offset is expected to drive the photogenerated electron-hole pair to the oppositely charged electrodes [27].

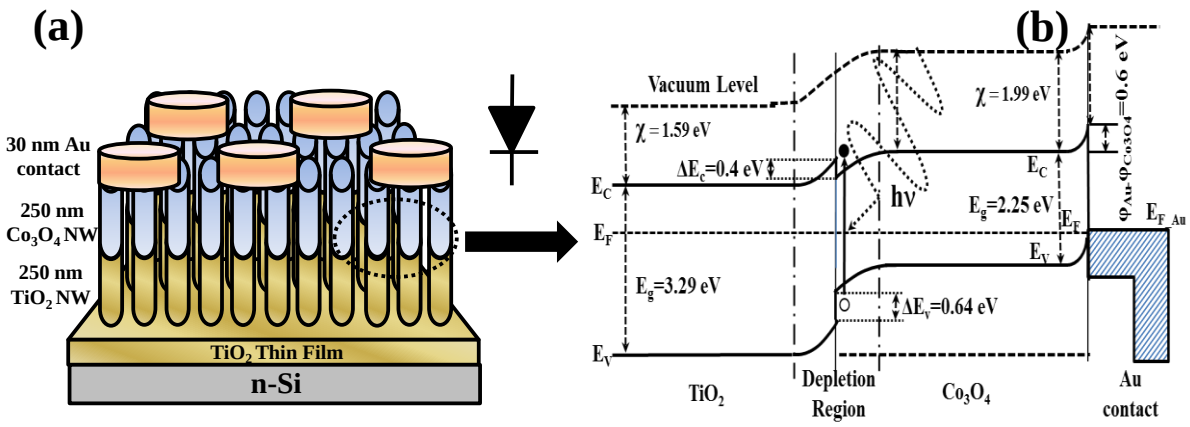

Fig. 4: (a) Schematic diagram of the prepared HND, (b) device band diagram at equilibrium

Fig.5a shows the current versus voltage (I-V) characteristic of the Au/Co_3O_4/TiO_2 HND at room temperature under dark and white light exposure. The forward bias is considered here as a positive DC voltage applied on the Au top electrode. The maximum rectifying ratio measured between -10 V to +10 V has a value of 2.26×10^2 at ± 3.4 V (Fig.5.a inset) which is 3.8 times superior to the reported value of 59 for ZnO/Si nano-heterojunction array [28]. A turn-on voltage of 1.5 V is recorded for dark, which reduced to 1 V under white light excitation. Large current was recorded for white light excitation, which may be due to barrier height lowering and multiple carriers generation. To understand the AC operation of the HND, we have measured the rectification efficiency under applied AC voltage with maximum ± 10 V at various frequencies from 200 Hz – 2 kHz. The output voltage vs time characteristics at 200 and 1000 Hz are displayed in Fig. 5b. A maximum efficiency of 7.77% was observed at 200 Hz frequency which gradually decreased with increase in signal frequency as shown in Fig. 5c. It is well known that the maximum efficiency for ideal diode halfwave rectifier is 40.6%. In our case, the low rectification efficiency is due to the presence of non-zero forward voltage drop [29]. Furthermore, it was observed that (Fig. 5b) with increase in frequency, the clipping abilities of the diode started deteriorating which may be due to the prominent reverse recovery transient related to the high frequency operation of

Co_3O_4/TiO_2 HND junction diode [30]. Hence our HND is suitable for low frequency operation.

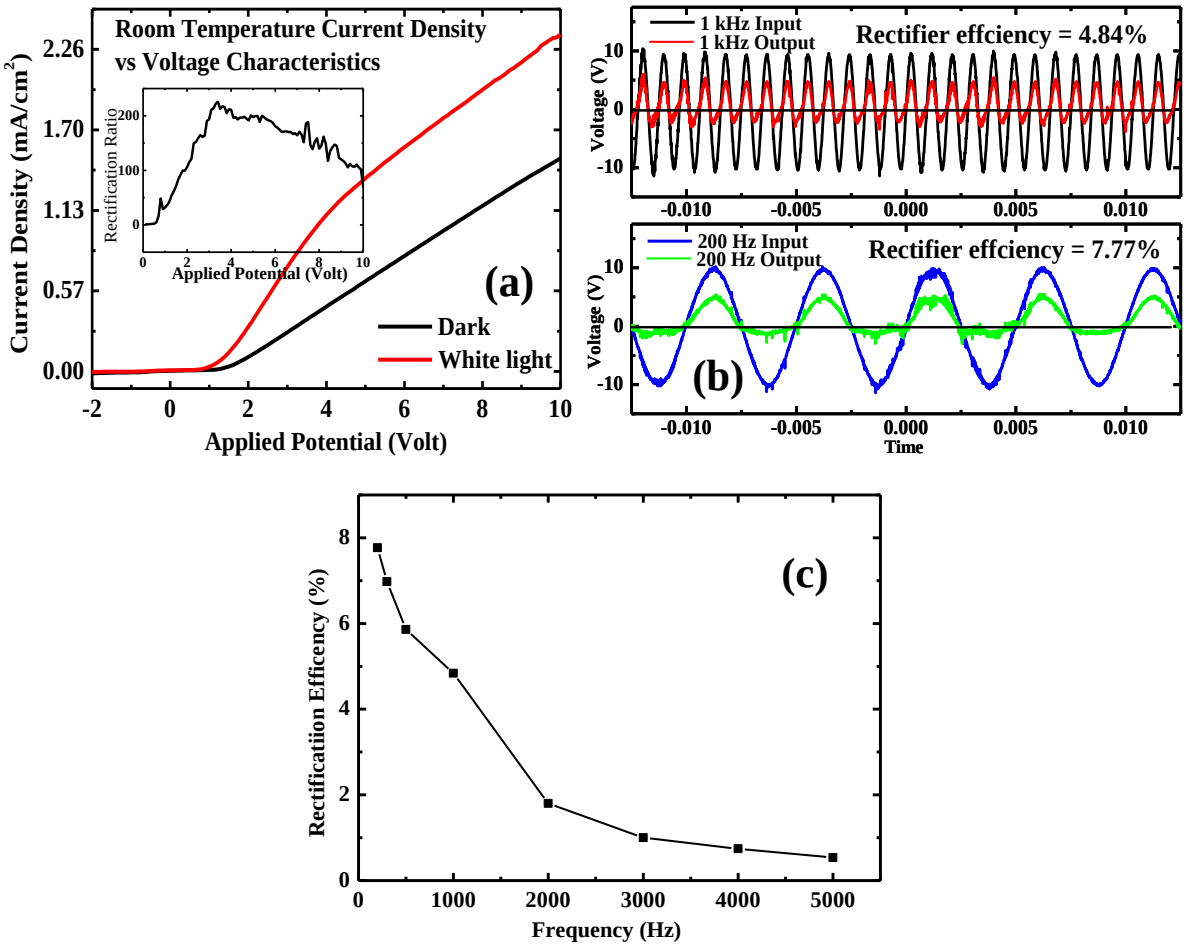

Fig. 5: (a) Room temperature current density-voltage characteristic under dark and white light illumination for Co_3O_4-TiO_2 NW device, inset shows the rectification ratio as a function of applied potential; (b) output and input characteristics comparison of half-wave rectifier at 200 and 1000 Hz; (c) Rectification efficiency-frequency spectrum for the heterostructure device.

The current density versus voltage (J-V) characteristics of the Au/Co_3O_4/TiO_2 HND at 50 K - 300 K are displayed in Fig. 6a. It can be clearly seen that with an increase in temperature there is an enhancement in the current through the diode. Averagely 6.87×10^2 times enhancement in current was achieved at 300 K compared with 50 K.

The ideality factor of the HND was calculated using the following formula at different temperatures [31]

$$n = \frac{q}{kT}\left(\frac{dV}{d(\ln(I))}\right), \quad (1)$$

where n=ideality factor; q=charge of electron; k=Boltzmann's constant; T=temperature; V= voltage; I= current through the HND

Fig. 6b shows the variation of the ideality factor with change in temperature from 50 K – 300 K. The ideality factor was observed to decrease with an increase in temperature. In the Co_3O_4 – TiO_2 HND the electrons gain more energy to cross the barrier height the temperature is increased. Hence, the effective barrier height is increased [32] resulting in an influence over the current transport along with thermionic emission [33]. Due to an increase in temperature, the energy difference between conduction band and Fermi level decreases resulting in an increase in flat band barrier [34,35]. Hence, a very high ideality factor (196) was observed at 50 K which gradually decreased with increase in temperature (15 at 300 K).

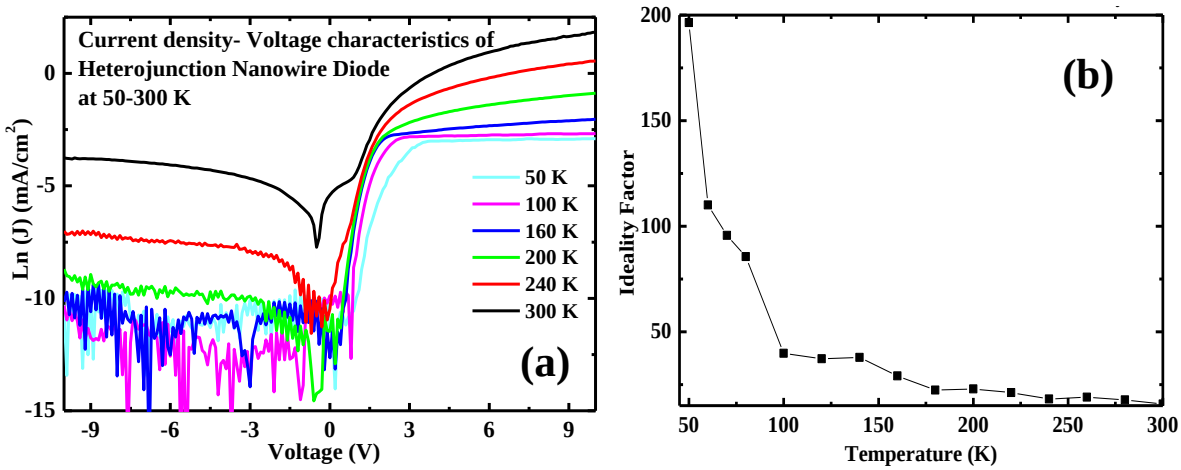

Fig. 6: (a) Current density-voltage characteristic for Co_3O_4-TiO_2 NW device at different temperatures from 50-300 K; (b) Ideality factor-temperature characteristic for Co_3O_4-TiO_2 NWs device

Fig. 7 shows the room temperature responsivity vs wavelength and internal gain vs wavelength spectra (inset) for Co_3O_4-TiO_2 HND at + 5 V applied bias. The internal gain was calculated using Eq. (2) [36].

$$G = \frac{h \times c \times R_\lambda}{\lambda \times \eta \times e} \tag{2}$$

where h = Planck's constant, c = speed of light, R_λ = responsivity, λ = wavelength of light, η = quantum efficiency ~1 and e = electron charge.

The maximum peak responsivity of 4.01 A/W and internal gain of 13.1 at 380 nm wavelength were due to the main band gap related transition in TiO_2 [16]. A small peak responsivity of 2.4 A/W and internal gain of 4.81 both at 620 nm wavelength were both due to main band gap related transition in Co_3O_4 [10].

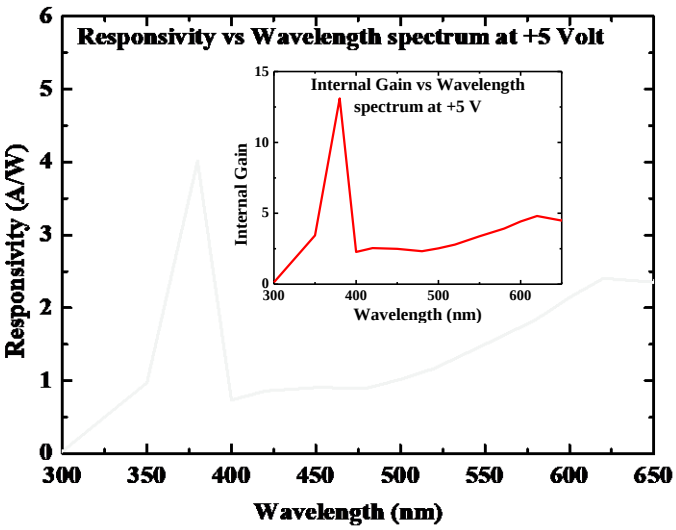

Fig. 7: Room temperature responsivity spectra at +5 V; inset shows the internal gain-wavelength spectrum at +5 V)

The detectivity and noise equivalent power (NEP) are two important parameters for a photodetector to evaluate its performance. Detectivity is given by

$$D^* = \frac{R_\lambda}{\sqrt{2eJ_{dark}}} \tag{3}$$

where J_{dark} is the dark current density.

The NEP is expressed as

$$NEP = \frac{\sqrt{A}\sqrt{B}}{D^*} \tag{4}$$

Where A is the area of the device (1.77×10^{-2} cm^2) and B is the bandwidth (1 kHz).

With these relations, detectivity and NEP were plotted as functions of operating voltage in a range of 3-7 V at 380 and 620 nm. These characteristics are displayed in Fig. 8. At 5 V, the detectivity was calculated to be 2.82×10^{11} and 1.69×10^{11} Jones under 380 and 620 nm wavelength photon illumination, respectively. The NEP at 5 V was estimated to be 14.9 and 24.8 pW under 380 and 620 nm photon illumination.

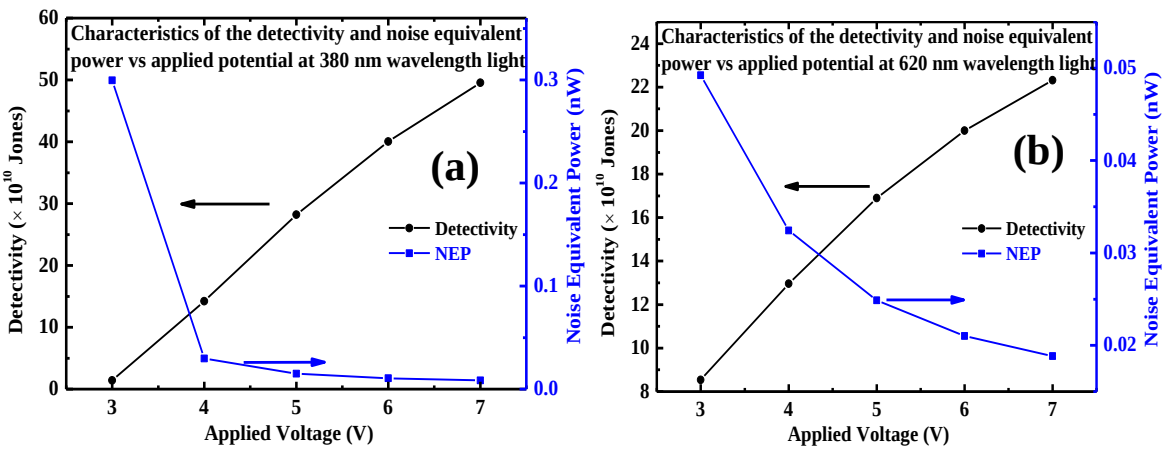

Fig. 8: Detectivity and noise equivalent power versus applied bias voltage characteristics under (a) 380 nm, (b) 620 nm wavelength illumination

Fig. 9a depicts the current density as a function of time under white light on/off switching irradiation at +5 V for the Co_3O_4 - TiO_2 HND. The rise and fall time were calculated using the following formulas [37]

$$I_{photo} = I_{dark} + A_1 [\exp(-\frac{t}{\tau_{1\_fall}})] + B_1 [\exp(-\frac{t}{\tau_{2\_fall}})] \tag{5}$$

$$I_{photo} = I_{dark} + A_2[1 - \exp(-\frac{t}{\tau_{1\_rise}})] + B_2[1 - \exp(-\frac{t}{\tau_{2\_rise}})] \quad (6)$$

where I_{photo} is photocurrent, I_{dark} is dark current, A_1, B_1, A_2 and B_2 are scaling constants, and τ_1 and τ_2 are the time constants. By fitting the photoresponse (Fig. 9b) using the mentioned equations, the time constants for decay were estimated to be τ_{1_fall}= 4×10^{-3} s and τ_{2_fall}= 0.25 s. For rise, the same parameters were estimated to be τ_{1_rise}= 3×10^{-3} s and τ_{2_rise}= 0.2 s. The time constant τ_{1_fall} and τ_{1_rise} may be associated with carrier generation and recombination in nanowires, and τ_{2_fall} and τ_{2_rise} may be related to the trapping and release process of carriers. [37]

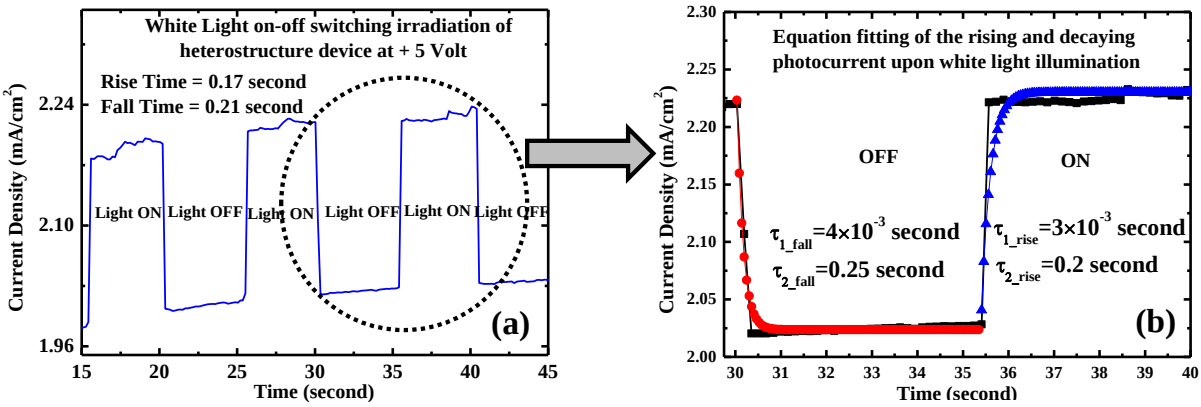

Fig. 9: (a) White light on-off switching irradiation of heterostructure device at +5 V; (b) Equation fitting of the rising and decaying photocurrent under white light illumination

4. Conclusion

In conclusion, we have prepared Co_3O_4 - TiO_2 HND using the GLAD technique. The TiO_2 exhibited a main band and sub-band related transitions at 3.29 and 2.75 eV, respectively. For Co_3O_4 a band to band and indirect band gap related transitions were observed at 2.25 and 1.6 eV. The HND showed a rectification ratio of 2.26×10^2 at ± 3.4 V. The turn on voltage of 1.5 V at dark was reduced to 1 V with light excitation. The rectification efficiency of the half-wave rectifier using the diode showed a decrease with an increase in operating frequency

having a maximum value of 7.77% at 200 Hz. At 380 nm wavelength, the maximum peak responsivity of 4.01 A/W and internal gain of 13.1 were recorded due to main band gap related transition in TiO_2. For Co_3O_4, at 620 nm wavelength excitation a small peak in responsivity of 2.4 A/W and internal gain of 4.81 were observed due to main band gap related transition. At 5 V, the detectivity was calculated to be 2.82×10^{11} and 1.69×10^{11} Jones under 380 and 620 nm wavelength photon illumination, respectively. The NEP at 5 V was estimated to be 14.9 and 24.8 pW under 380 and 620 nm wavelength photon illumination, respectively. From white light on-off switching, the rise and fall time were calculated to be 0.2 and 0.25 s. Therefore, the diode can be used as multiband detector for the detection of UV and visible light simultaneously.

Acknowledgement

The authors wish to thank Dr. Naorem Khelchand Singh, Dr. P. Chinnamuthu and Dr. Jay Chandra Dhar of NIT Nagaland, Department of Electronics and Communication Engineering for allowing the usage of electron-beam evaporation facility for sample fabrication. The authors would like to thank Dr. Ardhendu Saha of NIT Agartala, Department of Electrical Engineering for providing the optical absorption measurement facility. The authors acknowledge Dr. Sanjay Mondal and Mr. Rajesh Debnath of NIT Agartala, Department of Physics for providing the KBR press facility for pellet formation. The authors are grateful to SAIF, NEHU for TEM analysis. The authors wish to thank Dr. Sanatan Chattopadhyay and Mr. Abhishek Das of University of Calcutta, Centre for research in nanoscience and nanotechnology for EDX measurement. The authors are thankful to DST, Government of India and TEQIP-II, NIT Agartala, for financial support.

References

1. I. S. Cho, J. Choi, K. Zhang, S. J. Kim, M. J. Jeong, L. Cai, T. Park, X. Zheng, J. H. Park, Highly Efficient Solar Water Splitting from Transferred TiO_2 Nanotube Arrays, Nano Lett. 15 (2015) 5709–5715
2. S.-W. Cheong, Transition metal oxides: The exciting world of orbitals, Nat. Mater. 6 (2007) 927 - 928
3. X. Lang, A. Hirata, T. Fujita, M. Chen, Nanoporous metal/oxide hybrid electrodes for electrochemical supercapacitors, Nat. Nanotechnol. 6 (2011) 232–236
4. S. C. Das, R. J. Green, J. Podder, T. Z. Regier, G. S. Chang, A. Moewes, Band Gap Tuning in ZnO Through Ni Doping via Spray Pyrolysis, J. Phys. Chem. C, 117 (2013), 12745–12753
5. S. Ma, H. Liang, X. Wang, J. Zhou, L. Li, and C. Q Sun, Controlling the Band Gap of ZnO by Programmable Annealing, J. Phys. Chem. C 115 (2011) 20487–20490
6. L. J. Brillson, Y. Lu, ZnO Schottky barriers and Ohmic contacts, J. Appl. Phys. 109 (2011) 121301-1 – 121301-32
7. K.-I. Choi, H.-R. Kim, K.-M. Kim, D. Liu, G. Cao, J.-H. Lee, C_2H_5OH sensing characteristics of various Co_3O_4 nanostructures prepared by solvothermal reaction, Sensors and Actuators B 146 (2010) 183–189
8. H.-J. Kim, J.-H. Lee, highly sensitive and selective gas sensors using p-type oxide semiconductors: overview, Sens. Actuators, A 192 (2014) 607-627
9. L. Qiao, H. Y. Xiao, H. M. Meyer, J. N. Sun, C. M. Rouleau, A. A. Puretzky, D. B. Geohegan, I. N. Ivanov, M. Yoon, W. J. Weber, M. D. Biegalski, Nature of the band gap and origin of the electro-/photo-activity of Co_3O_4, J. Mater. Chem. C 1(2013) 4628-4633.

10. X. Zhu, J. Wang, D. Nguyen, J. Thomas, R. A. Norwood, N. Peyghambarian, Linear and nonlinear optical properties of Co_3O_4 nanoparticle-doped polyvinyl-alcohol thin films, Opt Mater Express 2 (2012) 103-110
11. V. Patil, P. Joshi, M. Chougule, S. Sen, Synthesis and Characterization of Co_3O_4 Thin Film, Soft Nanoscience Letters,, 2 (2012) 1-7
12. B. Fazio, P. Artoni, M. A. Iatì, C. D'Andrea, M. J. Lo Faro, S. Del Sorbo, S. Pirotta, P. G. Gucciardi, P. Musumeci, C. S. Vasi, R. Saija, M. Galli, F. Priolo, A. Irrera, Strongly enhanced light trapping in a two-dimensional silicon nanowire random fractal array, Light Sci. Appl. 5 (2016) e16062 1-7
13. R. B. Rakhi, W. Chen, D. Cha, H. N. Alshareef, Substrate Dependent Self-Organization of Mesoporous Cobalt Oxide Nanowires with Remarkable Pseudocapacitance, Nano Lett. 12 (2012) 2559–2567
14. L. Hu, Q. Peng, Y. Li, Selective Synthesis of Co_3O_4 Nanocrystal with Different Shape and Crystal Plane Effect on Catalytic Property for Methane Combustion, J. Am. Chem. Soc. 130 (2008) 16136–16137
15. K. J. Kim, Y. R. Park, Optical investigation of charge-transfer transitions in spinel Co_3O_4, Solid State Commun. 127 (2003) 25–28,
16. Z. Dong, Y. Fu, Q. Han, Y. Xu, H. Zhang, Synthesis and physical properties of Co_3O_4 nanowires, J. Phys. Chem. C 111 (2007) 18475–18478
17. Michael T. Taschuk, Matthew M. Hawkeye, Michael J. Brett, Glancing Angle Deposition in: Peter M. Martin (Eds.), Handbook of Deposition Technologies for Films and Coatings, William Andrew, Burlington Massachussets 2009, pp. 661
18. M. Xu, P. Da, H. Wu, D. Zhao, G. Zheng, Controlled Sn-Doping in TiO_2 Nanowire Photoanodes with Enhanced Photoelectrochemical Conversion, Nano Lett. 12 (2012) 1503 −1508

19. A. Lamberti, A. Chiodoni, N. Shahzad, S. Bianco, M. Quaglio, C. F. Pirri, Ultrafast Room-Temperature Crystallization of TiO_2 Nanotubes Exploiting Water-Vapor Treatment, Sci. Rep. 5 (2015) 7808 1-6
20. M. Pal, U. Pal, J. M. Gracia, Y. Jiménez, F. Pérez-Rodríguez, Effects of crystallization and dopant concentration on the emission behavior of TiO_2:Eu nanophosphors, Nanoscale Res. Lett. 7 (2012) 1-12
21. F. Z. Haque, R. Nandanwar, P. Singh, Evaluating photodegradation properties of anatase and rutile TiO_2 nanoparticles for organic compounds, Optik 128 (2017) 191–200
22. E. Redel, S. Petrov, Ö. Dag, J. Moir, C. Huai, P. Mirtchev, G. A. Ozin, Green Nanochemistry: Metal Oxide Nanoparticlesand Porous Thin Films from Bare Metal Powders, Small 8 (2012) 68–72
23. V.R. Shinde, S.B. Mahadik, T.P. Gujar, C.D. Lokhande, Supercapacitive cobalt oxide (Co_3O_4) thin films by spray pyrolysis, Appl. Surf. Sci. 252 (2006) 7487–7492
24. J. E. Moore, S. Dongaonkar, R. V. K. Chavali, M. A. Alam, M. S. Lundstrom, Correlation of Built-In Potential and I–V Crossover in Thin-Film Solar Cells, IEEE J. Photovoltaics 4 (2014) 1138 – 1148
25. T. F. Schulze, L. Korte, E. Conrad, M. Schmidt, B. Rech, Electrical transport mechanisms in a-Si:H/c-Si heterojunction solar cells, J. Appl. Phys. 107 (2010) 023711-1 - 023711-12
26. E. L. Uzunova, G. St. Nikolov, H. Mikosch, Electronic Structure and Vibrational Modes of Cobalt Oxide Clusters CoOn (n =1-4) and Their Monoanions, J. Phys. Chem. A 106 (2002) 4104-4114
27. A. J. Nozik, Nanoscience and Nanostructures for Photovoltaics and Solar Fuels, Nano Lett. 10 (2010) 2735-41

28. B. Yadian, H. Liu, Y. Wei, J. Wu, S. Zhang, L. Sun, C. Zhao, Q. Liu, R. V. Ramanujan, K. Zhou, C. L. Gan, Y. Huang, Towards Perfectly Ordered Novel ZnO/Si NanoHeterojunction Arrays, Small, 10 (2014) 344-348
29. P. A. Godoy, D. J. Perreault, J. L. Dawson, Outphasing Energy Recovery Amplifier With Resistance Compression for Improved Efficiency, IEEE Trans. Microwave Theory Tech. 57 (2009) 2895-2906
30. J. Maeng, M. Jo, S.-J. Kang, M.-K. Kwon, G. Jo, T.-W. Kim, J. Seo, H. Hwang, D.-Y. Kim, S.-J. Park, T. Lee, Transient reverse current phenomenon in a p- n heterojunction comprised of poly(3,4-ethylene-dioxythiophene):poly(styrene-sulfonate) and ZnO nanowall, Appl. Phys. Lett. 93, (2008) 123109-1 – 123109-3
31. S. K. Tripathi, Temperature-dependent barrier height in CdSe Schottky diode, J Mater Sci 45 (2010) 5468–5471
32. I. Hussain, M. Y. Soomro, N. Bano, O. Nur, M. Willander, Systematic study of interface trap and barrier inhomogeneities using I-V-T characteristics of Au/ZnO nanorods Schottky diode, J. Appl. Phys.113, (2013) 234509-1 -234509-6
33. S Karadeniz, M Sahin, N Tugluoglu, H Safak, Temperature-dependent barrier characteristics of Ag /p-SnS Schottky barrier diodes, Semicond. Sci. Technol. 19 (2004) 1098–1103
34. M.K. Hudait, S.B. Krupanidhi, Doping dependence of the barrier height and ideality factor of Au/n-GaAs Schottky diodes at low temperatures, Physica B 307 (2001) 125–137
35. K. Al-Heuseen, M. R. Hashim, Temperature-Dependent Barrier Characteristics of Inhomogeneous Pd/n-GaN Schottky Barrier, International Journal of Mathematical, Computational, Physical, Electrical and Computer Engineering 8 (2014) 633-637

36. O.M. Nayfeh, S. Rao, A. Smith, J. Therrien, M.H. Nayfeh, Thin Film Silicon Nanoparticle UV Photodetector, IEEE Photon Tech L 16 (2004) 1927-1929
37. Z. Jin, L. Gao, Q. Zhou, J. Wang, High-performance flexible ultraviolet photoconductors based on solution-processed ultrathin ZnO/Au nanoparticle composite films, Sci. Rep. 4 (2014) 4268-1 - 4268-8